

Observations of the Spin Period Variations of Inactive Box-wing Geosynchronous Satellites

Mr. Michael A. Earl¹ and Dr. Gregg A. Wade²
Royal Military College of Canada, Kingston, Ontario, Canada, K7K 7B4

Ground-based broadband photometric observations of four inactive geosynchronous satellites of "box-wing" design were frequently performed between March 2012 and December 2013 to commence a long-term study of their attitude dynamics. The brightness of the satellites was observed to vary in a periodic fashion, which was interpreted to mean that reflected sunlight was being modulated due to satellite spin. The average observed spin periods inferred from the light curves ranged from 158 seconds to 1548 seconds. The variation of each satellite's inferred spin period was observed to be small or negligible over hourly time scales, but varied significantly (from 15% to 25% of the average) and smoothly (possibly cyclically) over monthly to yearly time scales. The characteristics of the observed spin period variations, including the amplitudes, time scales, and shapes, differ greatly between satellites and suggest a relationship between the average observed spin period and the variation amplitude. The observed spin period variations were interpreted as being due to one or more external disturbance torques acting on the spacecraft. The most significant torque was found to be solar radiation pressure acting on the large-area solar panels. The magnitude of this torque produced sufficient angular accelerations to explain the observed spin period variations. A first-order phenomenological model is proposed to explain the high level aspects of the observed phenomena.

¹PhD Candidate, Department of Physics, Royal Military College of Canada, P.O. Box 17000 Station Forces Kingston, Ontario, Canada, K7K 7B4.

²Professor, Department of Physics, Royal Military College of Canada, P.O. Box 17000 Station Forces Kingston, Ontario, Canada, K7K 7B4.

keywords - geosynchronous, inactive, box-wing, satellite, resident space object, spin period, solar radiation pressure, torque, light curve, angular acceleration, spin period variation, space surveillance, space situational awareness, satellite rescue mission, spacecraft characterization, precession, synodic period, ground-based optical, broadband photometry, photometric analysis, electro-optical satellite surveillance, Solidaridad, Telstar, Echostar, Asiasat 3, HGS-1, PAS-22, moment of inertia, solar panel

Nomenclature

%	= percentage	
#	= catalog number	
°	= units: degrees of arc	
'	= units: minutes of arc (arc-minutes)	
''	= units: seconds or arc (arc-seconds)	
A	= amplitude of spin period variation	(s)
A_{panel}	= area of a single solar panel	(m ²)
a	= length of satellite central box (cube) side	(m)
α	= equatorial right ascension coordinate	(°)
α_+	= angular acceleration assisting spin	($\mu\text{rad} \cdot \text{s}^{-1} \cdot \text{day}^{-1}$)
α_-	= angular acceleration opposing spin	($\mu\text{rad} \cdot \text{s}^{-1} \cdot \text{day}^{-1}$)
α_{HGSmax}	= maximum observed angular acceleration of HGS-1	($\mu\text{rad} \cdot \text{s}^{-1} \cdot \text{day}^{-1}$)
α_{mag}	= angular acceleration due to magnetic field torque	($\mu\text{rad} \cdot \text{s}^{-1} \cdot \text{day}^{-1}$)
α_{spin}	= net spin angular acceleration	($\mu\text{rad} \cdot \text{s}^{-1} \cdot \text{day}^{-1}$)
α_{SRP}	= angular acceleration due to solar radiation pressure torque	($\mu\text{rad} \cdot \text{s}^{-1} \cdot \text{day}^{-1}$)
α_{SRPmax}	= maximum angular acceleration due to solar radiation pressure torque	($\mu\text{rad} \cdot \text{s}^{-1} \cdot \text{day}^{-1}$)
°C	= units: degrees Celsius	
D	= residual dipole moment	(A · m ²)
d	= units: days of time	
Δt	= difference in time	(s)
δ	= equatorial declination coordinate	(°)
θ_1	= reference angle 1	(rad)
θ_2	= reference angle 2	(rad)
θ_3	= reference angle 3	(rad)
I	= moment of inertia	(kg · m ²)
l_{panel}	= length of a single fully deployed solar panel	(m)
l_{tot}	= total length of a satellite (wing span)	(m)

λ	= wavelength	(nm)
M	= total mass of satellite	(kg)
M_{Earth}	= magnetic moment of the Earth	(T · m ³)
m_{box}	= mass of the central satellite box (cube)	(kg)
m_{panel}	= mass of a single solar panel	(kg)
P_{rad}	= average solar radiation pressure at 1 A.U. from the Sun	(Pa)
π	= fundamental constant (3.14159265359)	
q_1	= reflectivity of a solar panel side	
q_2	= reflectivity of the opposite solar panel side to q_1	
R	= distance from the center of the Earth	(m)
s	= units: seconds of time	
T	= satellite spin period	(s)
\bar{T}	= average satellite spin period	(s)
T_1	= observed satellite spin period at one specific epoch	(s)
T_2	= observed satellite spin period at an epoch later than T_1	(s)
T_{Earth}	= orbit period of the Earth	(days)
t	= day of year	(d)
t_0	= reference time that determines the phase parameter	(d)
t_1	= reference time 1	(s)
t_2	= reference time 2 (later than t_1)	(s)
t_3	= reference time 3 (later than t_2)	(s)
w_{panel}	= width of a single solar panel	(m)
y	= units: years of time	

I. Introduction

SPACECRAFT characterization is becoming an important component of resident space object (RSO) surveillance because of its potential advantages to the satellite industry and especially to the Defense Advanced Research Projects Agency (DARPA) (1). For instance, in the event that a vital spacecraft's attitude control is compromised, spacecraft characterization has the potential to determine the spacecraft's attitude and attitude dynamics in preparation for a ground-based or space-based (rendezvous) rescue mission. Although research has been conducted to explore the feasibility of space-based rescue missions (2), (1), very little research has been conducted to assess the short-term dynamics of inactive spacecraft prior to potential space-based rendezvous missions. Even less research has been conducted to explain the cause(s)

and predict the behavior of inactive spacecraft attitude dynamics over the long term.

Box-wing spacecraft have "wing spans" (total length, with solar panels) of up to 30 metres, and can have masses of up to 5,000 kg. In the absence of active attitude control, the spacecraft will be influenced by a variety of unbalanced torques. One consequence of these unbalanced torques is that the RSOs might begin to spin and therefore also precess. In the context of this paper, an 'inactive' RSO is a spacecraft without active attitude control, i.e. its attitude varies by natural means only.

Long term spin period variations of inactive GEO RSOs have been sparsely reported in the literature (3). The most significant investigation that studied the the long term (several years or more) apparent spin period variation of a number of inactive GEO RSOs, mainly Russian Raduga (rainbow) and Gorizont (horizon) types, was conducted by Papushev et al. of the Russian Institute of Solar Terrestrial Physics (ISTP) with the Sayan Solar Observatory (SSO) (3). Papushev et al. observed 20 inactive GEO RSO's from 1987 to 2004. Their research suggested that an inactive GEO RSO can have an observed average spin period between 10 seconds and 450 seconds (3). Their research also suggested that the spin period can vary by as much as 85% from the average over a time scale of several days to several years (3). Papushev et al. proposed reasons for these variations, including solar radiation pressure (SRP), magnetic force due to spacecraft plasma charges and micro-jets caused by tiny holes in the hermetic pressurized spacecraft cabins (3). However, they did not provide a torque source analysis to determine the primary cause.

More recently, optical surveys of inactive GEO RSO spin rates conducted by Binz et al. in 2012 at the U.S. Naval Research Laboratory (NRL) and Cognion in 2014 at Oceanit Laboratories, resulted in spin periods between 16.48 seconds (for GOES 8) (4) and 6000 seconds (for TDRS-4) (1). Cognion studied a decommissioned subset of the Geostationary Operational Environmental Satellites (GOES) that included GOES 8, 9, 10, 11, and 12 (4). Cognion concluded that the GOES satellites exhibited spin periods ranging from 16 seconds to 20 minutes and exhibited different light curves from one another, despite nearly identical satellite designs (4). Cognion hypothesized that on-orbit changes to some of the GOES satellites studied might explain these differing light curves (4).

The research presented in this paper describes the ground-based small-aperture broadband optical photometric observations of four inactive box-wing GEO RSOs conducted from March 3, 2012 to December 24, 2013. Table 1 lists the four RSOs. The electro-optical hardware used to obtain the observations is listed in Table 2. The observation sampling cadence was on average one data point every 3.32 ± 0.05 seconds. Light curves were produced from these photometric observations in order to determine apparent spin periods. Light curves of each RSO were frequently obtained (at least twice per week, weather permitting) to determine each RSO apparent spin period's rate of change over time.

³Space-Track: The source for space surveillance data: <https://www.space-track.org>.

Table 1 GEO RSOs chosen

NORAD #	COSPAR # ³	COMMON	OWNER	OBSERVATIONS	OBSERVATION TIME
22911	1993-073-A	Solidaridad 1	Mexico	40	06/16/12 - 11/03/13
22927	1993-077-A	Telstar 401	USA	56	03/05/12 - 12/24/13
24313	1996-055-A	Echostar 2	USA	62	03/11/12 - 09/23/13
25126	1997-086-A	HGS-1	USA	33	06/16/12 - 07/13/13

Table 2 Electro-optical hardware

HARDWARE	BRAND AND MODEL	SPECIFICATIONS
Optical Telescope	Celestron NexStar 11 GPS	Aperture: 0.28m (11 inches) Mount type: Fork equatorial
CCD Camera	Santa Barbara Instrument Group (SBIG) ST-9XE ⁴	Detector: Kodak KAF-0261E Array size: 512 x 512 pixels Pixel size: 20 μm (square) Quantum efficiency: 67% at $\lambda=600\text{nm}$ Chip cooling: 40°C below ambient
CCD Camera	SBIG ST-8XE ⁵	Detector: Kodak KAF-1603ME Array size: 1530 x 1020 pixels Pixel size: 9 μm (square) Quantum efficiency: 83% at $\lambda=640\text{nm}$ Chip cooling: 40°C below ambient

The primary goals of this research were to verify the general phenomena and conclusions reported by Papushev et al., to observe and measure the spin period variations of the chosen RSOs with a resolution of two or more data points per week per RSO (weather-permitting), to determine the RSOs' maximum apparent spin angular accelerations from spin period variation measurements, to verify the most likely disturbance torque that could cause the maximum apparent spin angular accelerations, to develop a preliminary hypothesis as to why an RSO's spin angular acceleration would appear to vary with time, and to develop a preliminary first-order model to explain the RSOs' apparent spin period behaviors.

II. Observations

All of the observations were conducted from Greater Napanee, Ontario, Canada (Longitude: $-76^{\circ} 53' 25''.8$, Latitude: $+44^{\circ} 07' 23''.8$, Altitude: 79m). This location was chosen because of its very low artificial light pollution levels. From this dark sky site, the maximum signal from each chosen RSO could be obtained.

⁴SBIG, Operating Manual: CCD Camera Models ST-7XE/XME, ST-8XE, ST-9XE, ST-10XE/XME and ST-674 2000XM/XCM With High Speed USB Interface, 1.4 ed., June 2004.

⁵Ibid.

A. Obtaining the Photometric Data

In most cases a continuous series of one-second CCD integration times was used over a time scale of between one and two hours. The telescope's sidereal tracking was switched off to prevent the RSO from streaking on the image plane. Each inactive RSO was allowed to drift across the field of view (FOV) until it reached an edge of the FOV. The telescope was then manually slewed so that the target RSO appeared on the opposite side of the FOV so that the RSO could slowly drift across the FOV once again. This routine was repeated as many times as required throughout each 1-2 hour observation session. The CCD automatically imaged during the entirety of each observation session and each image was automatically stored. No filters were used, i.e. broadband only, in order to allow the CCD to detect the maximum RSO signal and to allow the best possible sampling cadence.

Each CCD observation had a duty cycle of 3.32 ± 0.05 seconds. Some of the light curve maxima could be located within very brief specular reflections that can have very short durations (less than 10 seconds). In many of these cases the duty cycle was required to be the uncertainty of the CCD time tag values to make sure that the maximum was included.

Strict observation criteria were defined and followed to allow maximum RSO signal and minimum background signal. For example, images could only be obtained when the Sun's elevation was less than -12° (nautical twilight) and the Moon's phase (when above the local horizon) was less than 50%. The phase angle of the RSO had to be between 10° and 90° (to maximize RSO signal) and the RSO's elevation had to be greater than 15° to avoid excessive atmospheric signal absorption. The CCD detector chip's maximum temperature during observation was not to exceed -20°C to minimize dark (thermal) currents.

A single CCD image of the Telstar 401 inactive GEO RSO is shown in Fig. 1 to illustrate the image quality maintained throughout the research period. Within Fig. 1, the integration time was 1 second, the compass direction at upper left indicates the image's orientation, the RSO (indicated by its NORAD catalog number) appears as a small dot, and all of the small horizontal streaks are stars. With each subsequent image, Telstar 401 would appear to move slowly and nearly parallel to the declination (dec.) axis, unless the RSO was at its maximum or minimum dec.

B. Light Curve Generation

Each image of a GEO RSO represented a single photometric data point on a light curve. The photometric extraction method involved the location of the RSO's centroid within each image, the summation of the pixel brightness values that were greater than the average image background brightness and the subtraction of the average background brightness.

The photometric data extraction was automatically performed by MATLAB software developed by the

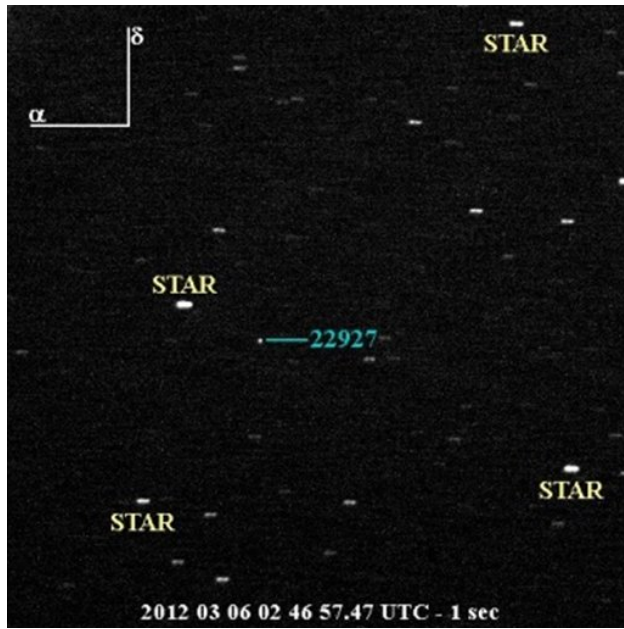


Fig. 1 Image of Telstar 401: 02:46:57 UTC March 6, 2012

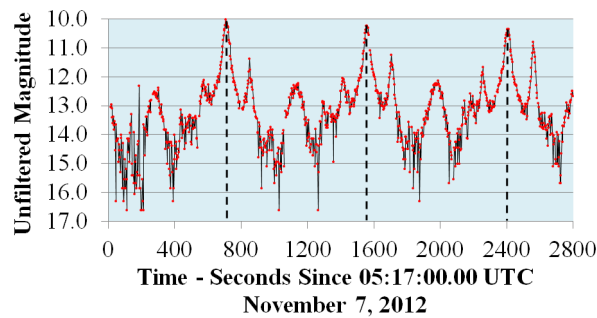
primary author. This software was designed to locate the RSO automatically within each image and extract the image time tag and the background-subtracted RSO signal.

Example light curves extracted from the photometric data are shown for Solidaridad 1 (Fig. 2(a)), Telstar 401 (Fig. 2(b)), Echostar 2 (Fig. 2(c)), and HGS-1 (Fig. 2(d)). Within each light curve shown, the dashed lines indicate similar light curve characteristics that were used for apparent spin period determination, and the time elapsed between two adjacent dashed lines is interpreted to be the approximate apparent spin period for the epoch date indicated. In all four cases the light curve appears to contain repeating characteristics suggesting a periodic behavior most likely due to the RSO spinning about an axis of rotation. All four of these light curves support the apparent periodic behavior observed by Papishev et al. (3).

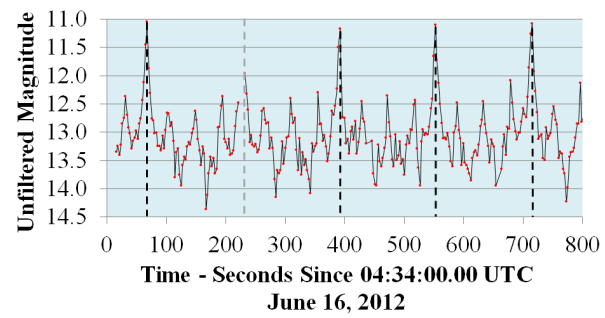
Despite the RSOs' similar box-wing designs, the light curves shown in Fig. 2(a) to Fig. 2(d) appear to have very diverse characteristics. These differences suggest that the RSOs had unique spin axis orientations and unique spin rates.

C. Determination of the Apparent Spin Period

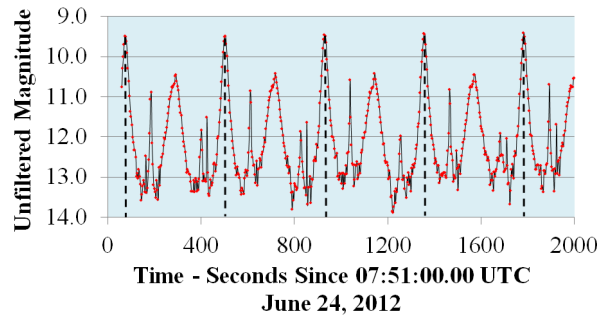
The apparent spin periods were estimated from the light curves, including those shown in Fig. 2, by measuring the time elapsed between similar light curve characteristics. At first, the apparent spin periods from all adjacent maxima pairs in a light curve were compared to determine whether or not the apparent spin period varied more than the measurement uncertainty (assumed to be the CCD duty cycle) during a single observation session (one to two hours). Telstar 401 and Echostar 2 were found to have negligible apparent spin period variations within a single light curve. Solidaridad 1 and HGS-1 (the RSOs with the



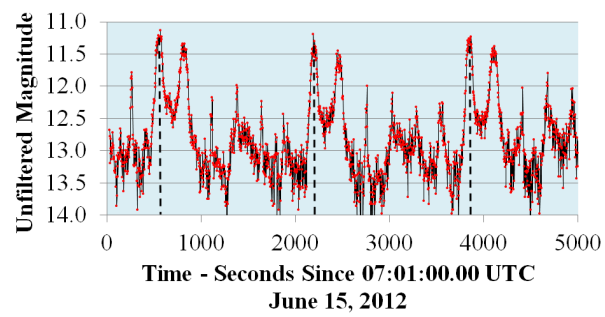
a) Solidaridad 1



b) Telstar 401



c) Echostar 2



d) HGS-1

Fig. 2 Example light curves

longest apparent spin periods of the four) were found to have highly varying apparent spin periods (up to 20 seconds variation) when comparing spin periods determined from adjacent maxima pairs. This was not the result of systematic error because none of the determined spin periods of Telstar 401 and Echostar 2 exhibited any significant variation in apparent spin period within several hours of observation.

When determining Telstar 401's and Echostar 2's apparent spin periods, the light curve's first and last maxima corresponding to the same light curve characteristic were chosen. The time corresponding to the first maximum was subtracted from the time corresponding to the last maximum and the time difference's uncertainty was determined by adding the two time uncertainties (each being the CCD's duty cycle) in quadrature. The resulting time duration was divided by the number of full observed periods between them to determine the apparent spin period with the minimum uncertainty. This process is illustrated in Fig. 3.

When determining Solidaridad 1's and HGS-1's apparent spin periods, the elapsed time between all adjacent maxima were measured and compared. The maximum and minimum apparent spin periods in a single light curve were averaged and the random uncertainty was deemed to be half of the difference between the maximum and minimum values.

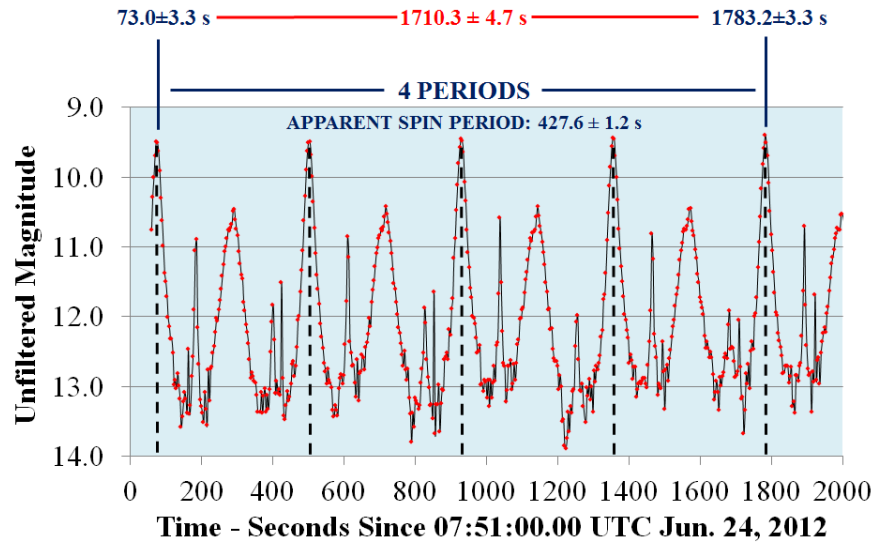
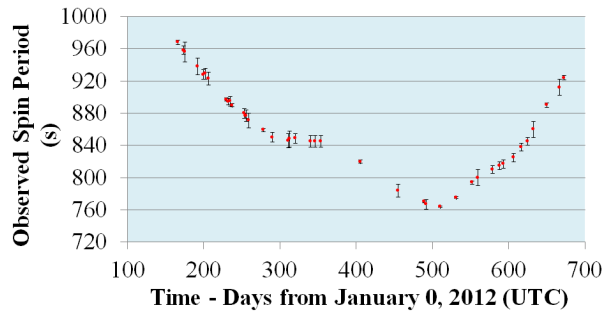


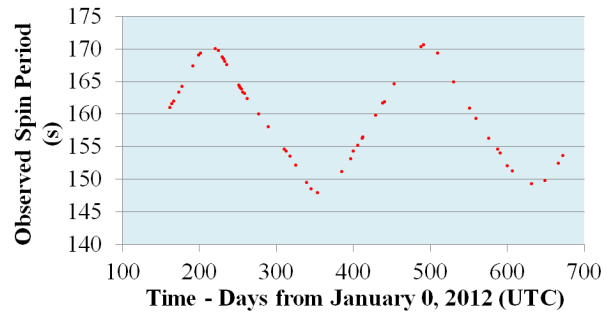
Fig. 3 Echostar 2's apparent spin period

D. Variations of the Observed Spin Periods

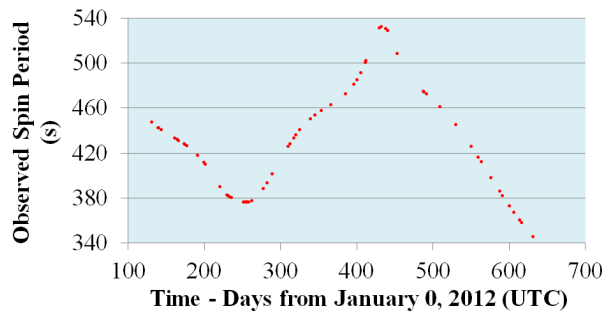
The apparent spin periods were determined from all light curves obtained. Plots of the apparent spin period measured versus the number of days elapsed since January 0, 2012 (December 31, 2011) are shown for Solidaridad 1 (Fig. 4(a)), for Telstar 401 (Fig. 4(b)), for Echostar 2 (Fig. 4(c)), and for HGS-1 (Fig. 4(d)). In all four cases the spin period appeared to vary secularly and smoothly with time.



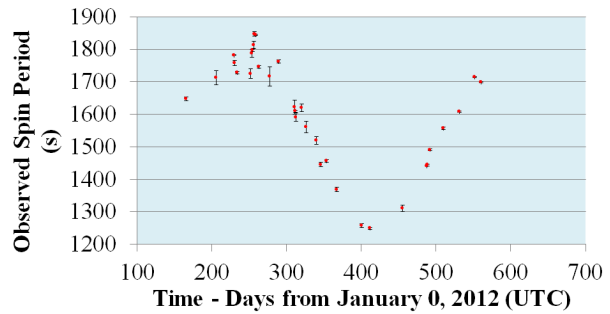
a) Solidaridad 1



b) Telstar 401



c) Echostar 2



d) HGS-1

Fig. 4 Observed spin period variations

The apparent spin period variations appeared different from each other in several distinct ways. The average apparent spin periods ranged from 158 seconds (for Telstar 401) to 1548 seconds (for HGS-1), as shown in Table 3. The cause of such a diverse range of average spin periods is currently unknown. However, these variations confirmed what Papushev et al. had observed for the Raduga and Gorizont RSOs (3) with the exception that the maximum observed spin period can be somewhat greater than 440 seconds. Table 3 demonstrates that the amplitude of the apparent spin period variation is different for each RSO. Figure 5 shows the amplitude of each RSO spin period variation plotted against its average observed spin period. Figure 5 suggests that the apparent spin period variation amplitude is dependent on the average apparent spin period. However, Fig. 4(a) and Fig. 4(d) suggest that Solidaridad’s and HGS-1’s full spin period variation amplitudes have not yet been observed, therefore more data is required to confirm this potential relationship. Echostar 2’s and Telstar 401’s apparent spin periods appear to vary in a cyclical fashion. Telstar 401’s apparent spin period variation appears to have a minimum period of approximately 280 days. Echostar 2’s apparent spin period variation appears to have a cycle period of at least 380 days. If Solidaridad 1’s apparent spin period variation is cyclical, then the cycle period appears to be greater than 520 days. If cyclical, HGS-1’s apparent spin period variation could have a cycle period greater than 320 days. The apparent spin period variations do not appear as simple sinusoids (if periodic). Telstar 401’s apparent spin period variation (Fig. 4(b)) appears quasi-sinusoidal. Echostar 2’s apparent spin period variation (Fig. 4(c)) would be similar to sinusoidal behavior if not for an inflection behavior between days 310 and 390 and between days 450 and 520 in which the magnitude of the slope levels out for some time before resuming its steeper behavior. Solidaridad 1’s apparent spin period variation (Fig. 4(a)) shows a similar inflection feature between days 280 and 380. HGS-1’s spin period appeared to vary within much smaller time frames. Between days 240 and 260, HGS-1’s spin period appeared to increase by 125 seconds in under 10 days. This behavior was unique among the four RSOs studied.

Table 3 The observed apparent spin period characteristics

RSO	Minimum Spin Period (s)	Maximum Spin Period (s)	Spin Period Amplitude (s)	Average Spin Period (s)	Variation Time Scale (d)
Solidaridad 1	764	968	204	866	>520
Telstar 401	145.0	170.6	25.6	157.8	280
Echostar 2	345.4	532.2	186.8	438.8	>380
HGS-1	1249	1847	598	1548	>320

All of the apparent spin period variations appear to be more complex than the lower-resolution observations, obtained by Papushev et al. for Raduga 12, Raduga 10, and Gorizont 9, would suggest (3). However, it might be possible that the Russian GEO RSO designs exhibit different apparent spin period variation

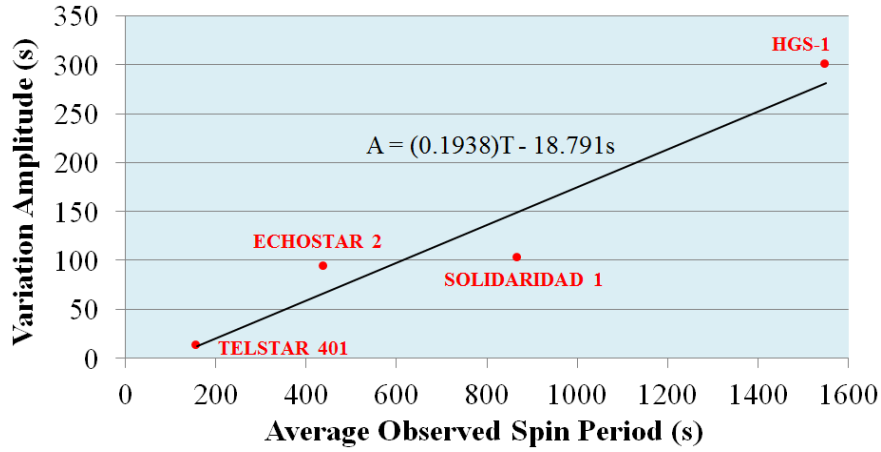


Fig. 5 Spin period variation amplitude vs. average observed spin period

behaviors than their North American counterparts.

The inflection feature appears to become more pronounced with increasing average apparent spin period. The plot of Telstar 401 (Fig. 4(b)) has very small inflections between days 260 and 300 and again between days 390 and 430. The plot of Echostar 2 (Fig. 4(c)) shows more pronounced inflections between the maximum and minimum apparent spin period. The plot of Solidaridad 1 (Fig. 4(a)) shows the most pronounced inflection before the first observed minimum spin period.

E. Observed Spin Angular Acceleration

The observed spin period variations suggest that each RSO's spin angular velocity is varying with time due to an external or an internal torque, as Papushev et al. had originally proposed (3). Using Eq. (1), the apparent spin angular accelerations of the RSOs were determined by using all chronologically adjacent spin period data points in Fig. 2(a) to Fig. 2(d) that were greater than 3 days apart and less than 10 days apart (Δt). The time coordinate for each angular acceleration data point was defined as the average of the two epoch times corresponding to the two spin period data points used in each determination.

$$\alpha_{spin} = \frac{2\pi}{\Delta t} \left[\frac{1}{T_2} - \frac{1}{T_1} \right] \quad (1)$$

The apparent angular acceleration vs. time is shown for Solidaridad 1 (Fig. 6(a)), for Telstar 401 (Fig. 6(b)), for Echostar 2 (Fig. 6(c)), and for HGS-1 (Fig. 6(d)).

Figure 6(a) suggests that Solidaridad 1 had the weakest angular acceleration during the observation period when compared to those of the other three RSOs.

Telstar 401's apparent angular acceleration suggests a quasi-periodic behavior, as its apparent spin period variation (Fig. 4(b)) does. However, about the maximum and minimum angular accelerations, the angular acceleration is nearly constant over time. Echostar 2's apparent angular acceleration also suggests periodic

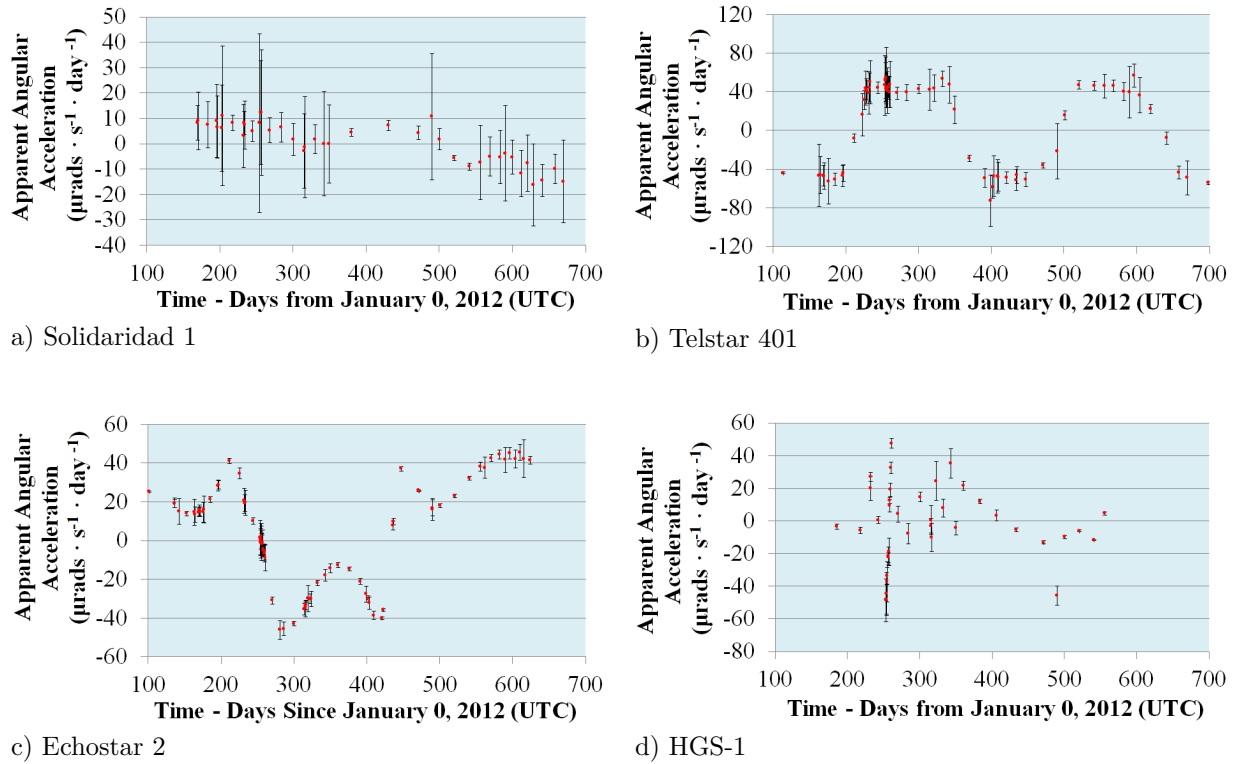


Fig. 6 Observed spin angular accelerations

behavior. HGS-1's apparent angular acceleration appears to be very erratic with a definite steep positive slope between days 250 and 260 in Fig. 6(d). Whether this sudden steep slope repeats or not is presently uncertain. Table 4 lists the maximum of each RSO's apparent angular acceleration magnitude.

Table 4 Maximum magnitudes of spin angular accelerations

RSO	Maximum Magnitude of Apparent Angular Acceleration ($\mu\text{rad} \cdot \text{s}^{-1} \cdot \text{day}^{-1}$)
Solidaridad 1	16 ± 16
Telstar 401	73 ± 27
Echostar 2	46 ± 5
HGS-1	49 ± 13

III. RSO Characteristics

In order to determine the most likely torque source that was causing the observed maximum spin angular accelerations shown in Table 4, the characteristics of each RSO (dimensions, mass, history) were carefully researched. This information was used to estimate the MOI (rotational inertia) of each RSO.

A. The "Box-wing" Spacecraft Design

The "box-wing" design consists of a central cube-shaped bus structure (the "box") and two large and flat rectangular solar panels (the "wings") connected to two opposite sides of the box, as illustrated in Fig. 7. The box portion has sides that are on average 2 to 3 metres in length. Each solar panel can be as long as 15 metres and as wide as 5 metres, depending on the power requirements.

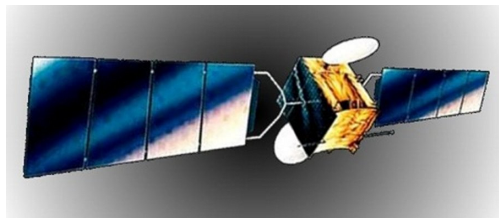


Fig. 7 Artist's conception of the "box-wing" design (Lockheed Martin)

B. History

Of the four RSOs, only one (HGS-1) was properly parked in the GEO graveyard orbit before deactivation. The basic characteristics of the RSOs are shown in Table 5.

Table 5 Basic characteristics of the chosen RSOs

CHARACTERISTIC	SOLIDARIDAD 1	TELSTAR 401	ECHOSTAR 2	HGS-1
Launch Date ⁶	Nov. 20, 1993	Dec. 16, 1993	Sep. 11, 1996	Dec. 24, 1997
Design ⁷	HS-601	AS-7000	AS-7000	HS-601HP
Designed Lifetime ⁸ (y)	14	15	12	15
Actual Lifetime (y)	6.75	3.1	11.8	4.5
Cause of Failure	Control Processor ⁹	Solar Storm (5)	Power Failure (6)	Depleted Fuel ¹⁰
Solar Panel Design	Black Silicon	Black Silicon	Black Silicon	Triple-Junction Gallium Arsenide

Solidaridad 1 (English: Solidarity) was a Mexican government telecommunications spacecraft constructed by Hughes Space and Communications (now called Boeing Satellite Systems)¹¹. Its lifetime was cut short by the failure of the main and backup satellite control processors (SCP) in 1999 and on August 27, 2000, respectively. The fault was blamed on short-circuits of the tin-plated electromagnetic relay caused by tin

⁶Space-track: The source for space surveillance data: <https://www.space-track.org>.

⁷G. D. Krebs, Gunter's space page: <http://space.skyrocket.de>.

⁸Ibid.

⁹NASA, Whisker failures: <http://nepp.nasa.gov/whisker/failures>.

¹⁰G. D. Krebs, Gunter's space page: Asiasat 3, 3s / HGS 1 / PAS 22: http://space.skyrocket.de/doc_sdat/asiasat-3.htm, 2013.

¹¹G. D. Krebs, Gunter's space page: Solidaridad 1, 2: http://space.skyrocket.de/doc_sdat/solidaridad-1.htm, 2014.

(solder) whisker growths¹².

Telstar 401 was an American commercial telecommunications payload constructed by Lockheed Martin for AT&T¹³. On January 11, 1997, the spacecraft suffered a catastrophic power failure which severed all communications with the ground. The cause of its malfunction was determined to be a solar coronal mass ejection (CME) which charged the spacecraft with high-energy ions (5), causing an electrical discharge¹⁴.

Echostar 2 was an American commercial telecommunications payload constructed by Lockheed Martin for the Echostar corporation and the Dish Network¹⁵. According to the Echostar corporation, on July 14, 2008, Echostar 2 "experienced a substantial failure that appears to have rendered the satellite a total loss." (7) This failure severed all communication between Echostar 2 and the ground stations, thus preventing its proper parking in the GEO graveyard orbit.

HGS-1's original name was "Asiasat 3"¹⁶. The payload was constructed by Hughes Space and Communications (now Boeing Satellite Systems) for the Asiasat corporation¹⁷. Launch was successful until the 4th stage malfunctioned, stranding the payload in a highly inclined and highly elliptical geostationary transfer orbit (GTO). The payload was declared a total loss by its insurers¹⁸.

Soon after its launch malfunction, Hughes decided to buy Asiasat 3 from the insurers. The payload was renamed "HGS-1" (Hughes-1 or Hughes Global Services 1). The payload did not have enough fuel to change its GTO orbit inclination; however the payload could be maneuvered so that the Moon's gravity could adjust the orbit inclination, thus providing an opportunity to place the payload into a geosynchronous orbit without having to deplete all of its station-keeping fuel (8).

Just six months after its initial launch, HGS-1 was successfully placed into a nearly circular geosynchronous orbit with an orbit inclination of approximately 11 degrees. When Hughes attempted to unfold the stowed solar panels after GEO insertion, only one successfully deployed, leaving the second one permanently stowed¹⁹.

Despite the solar panel deployment malfunction, the payload was active for approximately 3 years until it ran out of station-keeping fuel. The spacecraft was retired and parked in the GEO graveyard orbit in July 2002²⁰.

¹²NASA, Whisker failures: <http://nepp.nasa.gov/whisker/failures>.

¹³G. D. Krebs, Gunter's space page: Telstar 401, 402, 402R: http://space.skyrocket.de/doc_sdat/telstar-4.htm, 2014.

¹⁴G. D. Krebs, Gunter's space page: Telstar 401, 402, 402R: http://space.skyrocket.de/doc_sdat/telstar-4.htm, 2014.

¹⁵G. D. Krebs, Gunter's space page: Echostar 1, 2: http://space.skyrocket.de/doc_sdat/echostar-1.htm, 2014.

¹⁶G. D. Krebs, Gunter's space page: Asiasat 3, 3s / HGS 1 / PAS 22: http://space.skyrocket.de/doc_sdat/asiasat-3.htm, 2013.

¹⁷Ibid.

¹⁸Ibid.

¹⁹Ibid.

²⁰Ibid.

C. Dimensions and Masses

Obtaining any information concerning the exact component dimensions and masses of the RSOs proved to be very difficult. However, there was enough information available from accessible artist's conceptions to perform rough estimations of the dimensions and masses of the spacecraft bus (box) and solar panels (wings).

The compositions of Solidaridad 1, Telstar 401, and Echostar 2 were assumed to be a uniform density cube with two flat rectangular plates of identical uniform density attached to two opposite sides of the cube, as illustrated in Fig. 8. The composition of HGS-1 was assumed to be a uniform density cube with a single flat rectangular plate of uniform density (denoting the deployed panel) attached to one of the sides of the cube, and a single flat plate stowed against the cube's side opposite the deployed panel (denoting the un-deployed panel), as shown in Fig. 9. In both Fig. 8 and Fig. 9, 'CM' denotes the center of mass of each component. The cube was assumed to have sides of identical length 'a'. The artist's conceptions were used to determine the relative box and panel dimensions of each RSO, based solely on the scaling factor between the true wing span and the depicted wing span.

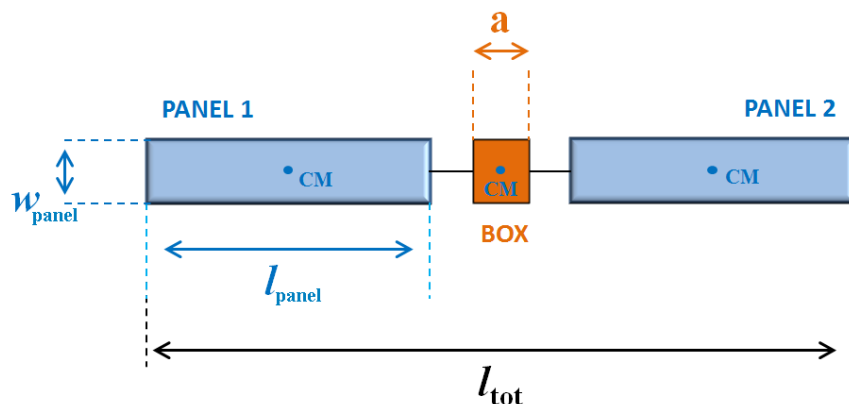


Fig. 8 Dimensions of Solidaridad 1, Telstar 401, and Echostar 2

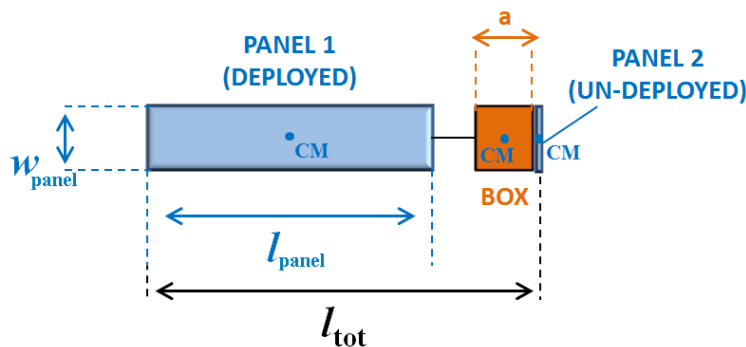


Fig. 9 Dimensions of HGS-1

Each RSO's wing span was assigned an arbitrarily chosen 0.5m uncertainty due to the references' lack

of RSO wing span uncertainties. The estimated component dimensions are listed in Table 6. HGS-1's, wing span was taken as the length from the un-deployed solar panel to the tip of the deployed solar panel, as shown in Fig. 9.

Published values of the components' masses were scarce in some references and contradictory in others. The masses quoted were normally on-orbit (beginning of life, BOL) masses, which were based on spacecraft with 100 percent of the maneuvering fuel on board, and the dry masses, which were based on spacecraft with no remaining maneuvering fuel on board. In the cases of Solidaridad 1, Telstar 401, and Echostar 2, the likely total spacecraft mass was neither the on-orbit mass value nor the dry mass value because they all had suddenly malfunctioned before they could be parked in the GEO graveyard orbit. Only HGS-1 had little to no maneuvering fuel remaining at its end of life (EOL). The masses of the communications dishes were assumed to be negligible when compared to the central box and the large solar panels.

The on-orbit mass and the dry mass quoted in the references were assigned an arbitrarily chosen 50kg uncertainty because the references did not state the uncertainties of either mass value. Each RSO's system center of mass was assumed to be located at the center of the box because the box mass was likely much larger than a panel mass.

In the cases of Solidaridad 1, Telstar 401, and Echostar 2, the spacecraft mass was estimated with the assumption that the maneuvering fuel consumption rate was uniform over the spacecraft's designed lifetime as listed in Table 5. The RSOs' true lifetimes from Table 5 were then used to estimate the fraction of fuel consumed when the RSO became inactive. This mass estimation assumed that the maneuvering thrusters did not fire at any time after the spacecraft malfunctioned. The total estimated mass of each RSO is listed in Table 6.

Solidaridad 1's total mass was estimated by subtracting the initial fuel mass at BOL²¹ from the on-orbit mass of a HS-601 design²². In the cases of Telstar 401 and Echostar 2, the total mass was estimated by subtracting the dry mass²³ from the initial on-orbit mass²⁴. The remaining fuel mass was estimated by assuming a uniform fuel use over the corresponding designed lifetime.

The mass of a single solar panel was estimated from its estimated area and its area density (9), depending on the panel material (shown in Table 5). The box mass was determined from the difference of the estimated total spacecraft mass and the estimated total solar panel mass. The resultant estimated single solar panel mass and the central box mass for each RSO are listed in Table 6.

²¹G. D. Krebs, Gunter's space page: Solidaridad 1, 2: http://space.skyrocket.de/doc_sdat/solidaridad-1.htm, (2014).

²²Encyclopedia Astronautica: HS 601: <http://www.astronautix.com/craft/hs601.htm>, (2010).

²³Ricardo's Geo-orbit Quick-look: Echostar 2 Specs: Western Hemisphere list: <http://www.geoorbit.org/westhemipgs/fecho2specp.html>, (2001).

²⁴G. D. Krebs, Gunter's space page: Echostar 1, 2: http://space.skyrocket.de/doc_sdat/echostar-1.htm, (2014).

The estimated wing span and dimensions of HGS-1's individual solar panels, assuming one deployed solar panel and one un-deployed solar panel, are listed in Table 7.

D. Moments of Inertia

A MOI estimation was required to determine the most likely disturbance torque(s) that caused the maximum apparent spin accelerations shown in Table 4. An 'end over end' spin rotation axis, illustrated in Fig. 10, was assumed. The MOI of each RSO was defined with a principal axis that was assumed to be coexistent with the spin axis shown in Fig. 10.

Equation (2) was used to estimate the MOIs of Solidaridad 1, Telstar 401, and Echostar 2. Equation (3) was used to estimate HGS-1's MOI. The total estimated MOIs are listed in Table 8.

Table 6 Estimated dimensions and masses of RSO components

CHARACTERISTIC	SOLIDARIDAD 1	TELSTAR 401	EHOSTAR 2	HGS-1
Wing Span (m)	21.0±0.5 ²⁵	23.9±0.5 ²⁶	23.9±0.5 ²⁷	26.2±0.5 ²⁸
Panel Length (m)	7.9±0.2	8.5±0.2	8.5±0.2	10.3±0.2
Panel Width (m)	2.0±0.1	3.1±0.1	3.1±0.1	2.3±0.1
Panel Area (m ²)	16±1	26±1	26±1	23±1
Box Side Length (m)	2.5±0.2	2.3±0.2	2.3±0.2	2.4±0.2
Total Mass (kg)	1980±70	2710±80	2020±80	1670±80 ²⁹
Box Mass (kg)	1910±70	2590±80	1900±80	1540±80
Panel Mass (kg)	36±2	60±2	60±2	64±2

Table 7 HGS-1's true wing span and estimated solar panel dimensions

CHARACTERISTIC	VALUE
True Wing Span (m)	14.4±0.3
Deployed Panel Length (m)	10.3±0.2
Deployed Panel Width (m)	2.3±0.1
Un-deployed Panel Length (m)	2.6±0.1
Un-deployed Panel Width (m)	2.3±0.1

$$I = \frac{1}{6} \{ m_{box} a^2 + m_{panel} [4l_{panel}^2 + 3l_{tot} (l_{tot} - 2l_{panel})] \} \quad (2)$$

²⁵G. D. Krebs, Gunter's space page: Solidaridad 1, 2: http://space.skyrocket.de/doc_sdat/solidaridad-1.htm, 2014.

²⁶Ricardo's Geo-orbit Quick-look: Echostar 2 Specs: Western Hemisphere list: <http://www.geoorbit.org/westhemipgs/fecho2specp.html>, 2001.

²⁷Ibid.

²⁸The Satellite Encyclopedia: Asiasat 3: <http://archive.today/e5c9>, September 2012.

²⁹Dry mass: The Satellite Encyclopedia: Asiasat 3: http://www.tbs-satellite.com/tse/online/sat_asiasat_3.html, 2014.

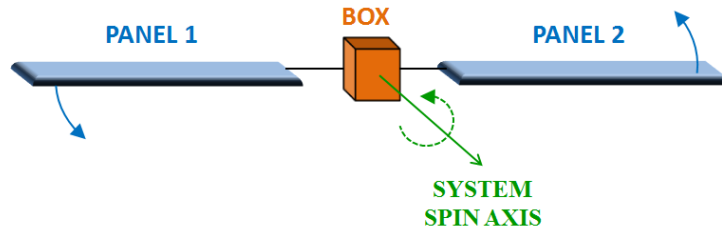


Fig. 10 Assumed spin axis

$$I = \frac{1}{6}m_{box}a^2 + m_{panel} \left[l_{tot}^2 + \frac{65}{192}l_{panel}^2 + (a + l_{panel}) \left(\frac{1}{2}a - l_{tot} \right) \right] \quad (3)$$

Table 8 Estimated MOIs

RSO	MOI (kg · m ²)
Solidaridad 1	5450±610
Telstar 401	10120±920
Echostar 2	9510±870
HGS-1	6320±520

IV. Analysis

A. Torque Source Evaluation

There are four primary natural external disturbance torques that can change the attitude of an RSO. Aerodynamic torque (based on atmospheric drag) acts on an RSO's cross-sectional areas. Magnetic (Lorentz) torque is the result of charged surfaces on the RSO, mainly due to solar ions, attempting to align it with the Earth's magnetic field. Gravity gradient torque attempts to stabilize an RSO's attitude by aligning it with the Earth's gravity well. SRP torque, primarily due to sunlight, acts on all sunlit parts of the RSO (10).

Since a GEO RSO is on average nearly 36,000 km in altitude, the aerodynamic and magnetic torques were considered to be negligible.

Gravity gradient torque acts to stabilize an RSO's attitude if the RSO is Earth-oriented. However, gravity gradient torque is cyclical over an RSO orbit (10). None of the observed spin period variations showed any evidence of periodic behavior within a single GEO orbit period. The spin period variation appeared to be secular in all four cases, which would suggest that gravity gradient torque could not be a viable contender.

In contrast to the aerodynamic, gravity gradient, and magnetic torques, the SRP torque will constantly act on an RSO no matter what its orbit altitude, with the exception of eclipses (10). As the Earth orbits the Sun, the RSO's spin axis will change its orientation with respect to the Sun, thereby modulating the SRP effect and possibly causing the observed spin period to change with time.

1. SRP Torque

In the case of HGS-1, the maximum instantaneous angular acceleration magnitude would have been experienced when its single deployed solar panel had been orthogonal to the SRP, as illustrated in Fig. 11. For this particular case, the maximum instantaneous SRP acceleration's magnitude was estimated with Eq. (4) (10). The average solar radiation pressure at 1 AU from the Sun was assumed to be 4.537×10^{-6} Pa.

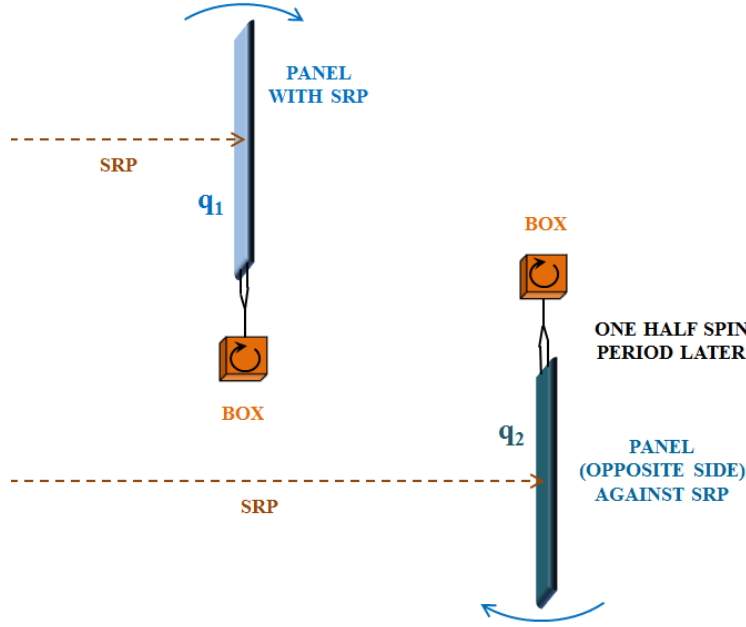


Fig. 11 SRP orthogonal to HGS-1's deployed solar panel

$$\alpha_{SRPmax} = \frac{P_{rad} A_{panel} (1 + q_1) (l_{tot} - l_{panel})}{2I} \quad (4)$$

The hypothetical maximum SRP angular accelerations for all four of the RSOs, assuming that all of the RSOs had a single deployed solar panel, were determined and the results are shown in Table 9. If these angular accelerations had been less than the observed maximum angular accelerations (shown in Table 4), then SRP could not be the cause of the observed maximum angular accelerations, no matter the orientation of the double solar panel RSOs with respect to the Sun.

Table 9 Observed and SRP maximum angular accelerations

SOURCE	SOLIDARIDAD 1	TELSTAR 401	EHOSTAR 2	HGS-1
Observed Maximum Absolute Angular Acceleration ($\mu\text{rad} \cdot \text{s}^{-1} \cdot \text{d}^{-1}$)	16±16	73±27	46±5	49±13
SRP Maximum Angular Acceleration ($\mu\text{rad} \cdot \text{s}^{-1} \cdot \text{d}^{-1}$)	11300	11600	12400	17000

V. First-order SRP Torque Variation Models

A. Net Angular Acceleration over a Single Spin Period

During a single spin period, the RSO's solar panel normal will constantly change its angle with respect to the SRP. Throughout half of the RSO's spin period, the SRP will ideally range in incidence angle from $-\pi/2$ radians to $\pi/2$ radians with the solar panel, with 0 radians representing orthogonality. Figure 12 depicts the solar panel orientation at three different times during the half spin period. At t_1 (left), a solar panel side is emerging into sunlight and has an oblique solar incidence angle (θ_1). At t_2 (center), the same panel side is orthogonal to the sunlight ($\theta_2=0^\circ$). At t_3 (right), the same panel side is nearly exiting sunlight and has an oblique solar incidence angle (θ_3). Assuming the SRP angular acceleration increased the spin angular velocity over this entire half spin period, the expression of the total angular acceleration over this half spin period was determined with the integral shown in Eq. (5) (where T is the RSO's spin period) and the resulting equation shown in Eq. (6).

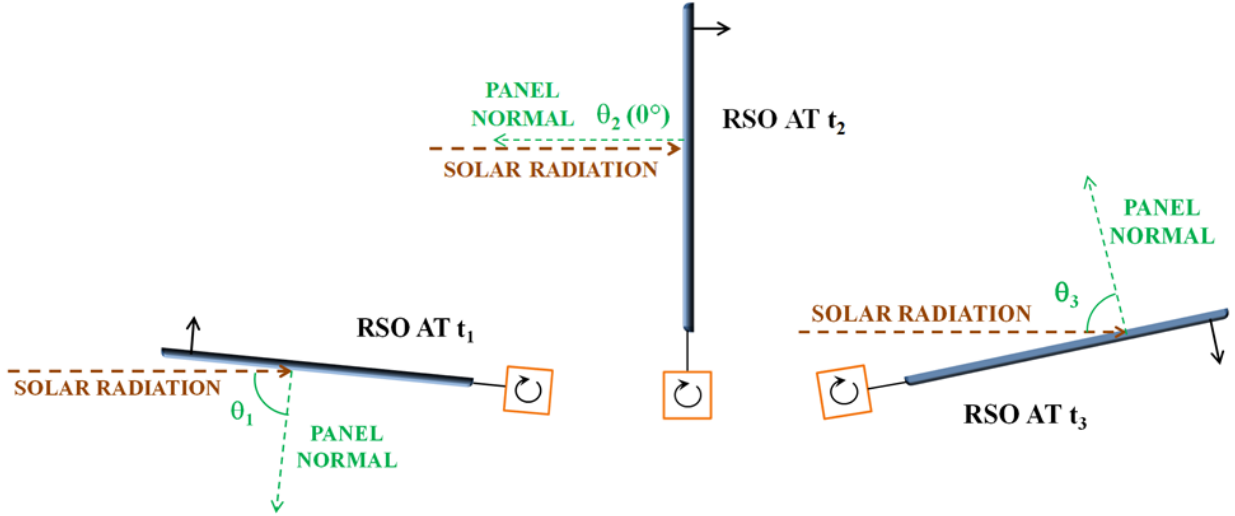


Fig. 12 Panel normal's solar incidence angle during half spin period

$$\alpha_+ = \frac{2P_{rad}A_{panel}(1+q_1)(l_{tot}-l_{panel})}{TI} \int_0^{\frac{T}{4}} \cos \left[2\pi \frac{t}{T} \right] dt \quad (5)$$

$$\alpha_+ = \frac{P_{rad}A_{panel}(1+q_1)(l_{tot}-l_{panel})}{I\pi} \quad (6)$$

During the remaining half of the spin period, the angular acceleration against the RSO's spin will decrease the spin angular velocity, thus negating some, all or more than the angular velocity that had been gained during the first half of the spin period. Assuming that the reflectivities of the panel sides were different from one another, with reflectivity of q_1 and q_2 , the net angular acceleration over one complete spin period was

determined with Eq. (7).

$$\alpha_+ + \alpha_- = \frac{P_{rad}A_{panel}(l_{tot} - l_{panel})|q_2 - q_1|}{I\pi} \quad (7)$$

HGS-1's net angular acceleration was assumed to be its maximum observed angular acceleration shown in Table 4. The difference between the two reflectivities was then estimated with Eq. (8), which is simply a rearrangement of Eq. (7).

$$|q_2 - q_1| = \frac{(\alpha_{HGSmax})I\pi}{P_{rad}A_{panel}(l_{tot} - l_{panel})} \quad (8)$$

The absolute reflectivity difference for HGS-1's deployed solar panel sides was estimated to be 0.0068. Assuming that q_1 was 0.5, the ratio of q_2 to q_1 was estimated to be 0.986. This calculation demonstrated that the two sides of HGS-1's solar panel had to have very similar reflectivities in order for the net spin angular acceleration to be the same as HGS-1's maximum observed angular acceleration (Table 4).

If an RSO with two deployed solar panels is being observed, it would likely be important to consider the relative orientation of these panels. If one panel has a (even slightly) different orientation relative to the other panel, then it is likely that a net SRP torque will act on the spacecraft that will assist or oppose the spin's angular velocity. This hypothesis is based on the very similar relative reflectivity of the two sides of a single panel, as shown above.

B. Cyclical Variation of Sunlight Incidence Angles over Earth Orbit Time Scales

Over one day, the sunlight incidence angle to a solar panel will change in a manner similar to Fig. 12 with each spin period. However, as the Earth orbits the Sun, an RSO's spin axis orientation with respect to the sunlight will slowly vary, as illustrated for an RSO with a single deployed solar panel in Fig. 13. Assuming that the RSO spin axis remains fixed in inertial space (no precession), the period of the sunlight variation will hypothetically be the Earth's orbit period (365.2422 days). Therefore, HGS-1's spin angular acceleration over one spin period within a sidereal year is predicted as shown in Eq. (9), where t_0 is a reference time at which the panel is orthogonal to the SRP and the net angular acceleration over one spin period is positive (increasing the spin's angular velocity).

$$\alpha_{spin} = \frac{P_{rad}A_{panel}(l_{tot} - l_{panel})|q_2 - q_1| \cos \left[\frac{2\pi(t-t_0)}{T_{Earth}} \right]}{I\pi} \quad (9)$$

Equation (9) suggests that there should exist two occurrences during the Earth's orbit when the RSO's angular acceleration is zero. These occurrences could correspond to the solar panel being edge-on to the sunlight. Figure 4(d) shows two extrema (a minimum and a maximum) of HGS-1's spin period, each

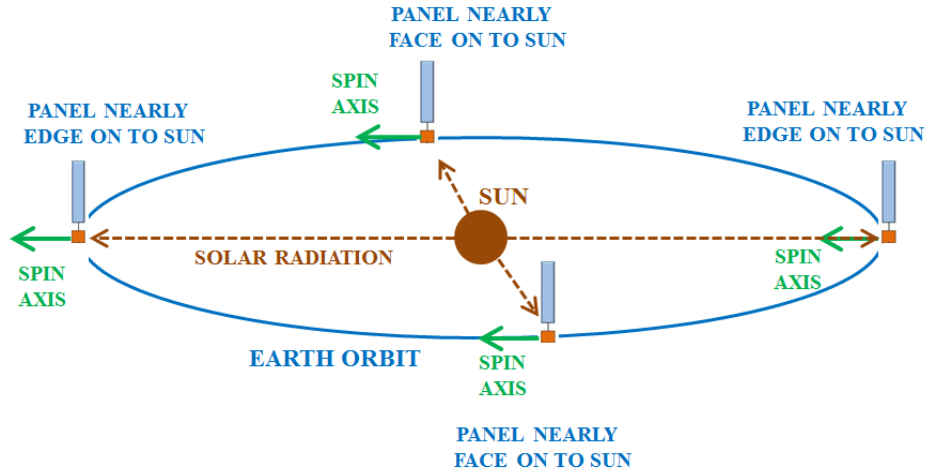


Fig. 13 Varying solar incidence angle on a solar panel over sidereal year

corresponding to an angular acceleration of zero.

The expression in Eq. (9) was integrated to predict the spin period variation of HGS-1 over the observation times. The constant of integration was the average observed angular velocity calculated from the maximum and minimum observed spin periods. In this case, the absolute reflectivity difference of 0.0068 resulted in spin periods that were several times greater than those observed. Assuming that the MOI and the panel dimensions of HGS-1 were correct, the only free parameters are the absolute reflectivity difference ($|q_2 - q_1|$) and the phase parameter (t_0). These free parameters were adjusted until the predicted spin period variation amplitude and phase approximately matched those of the observations. The value of the absolute reflectivity difference and phase parameter that allowed the best fit were 0.0019 and -30 days, respectively.

Figures 14(a) and 14(b) show the comparisons of the predicted and the observed spin angular acceleration variation and spin period variation of HGS-1. The dashed lines correspond to the predicted angular acceleration behavior and the predicted spin period behavior assuming an absolute reflectivity difference of 0.0019 and a phase parameter of -30 days. The dots represent the observed angular acceleration (from Fig. 6(d)) and the observed spin periods (from Fig. 4(b)). Figure 14(b) suggests that a possible apparent period of HGS-1's spin period variation is somewhat less than one sidereal year. The model does not adequately predict the sporadic behavior of the observed angular acceleration. However, the model does reproduce the angular acceleration variation amplitude's order of magnitude and some of the quasi-sinusoidal characteristics, especially between days 350 and 550. The predicted spin period variation is clearly satisfactory when considering that a first-order phenomenological model was used.

Equation (9) was only valid for HGS-1 because it assumed a single deployed solar panel. Solidaridad 1, Telstar 401, and Echostar 2 all have two deployed solar panels and therefore their dynamics have an extra layer of complexity. Not only could each side of the two solar panels have a different reflectivity, but they

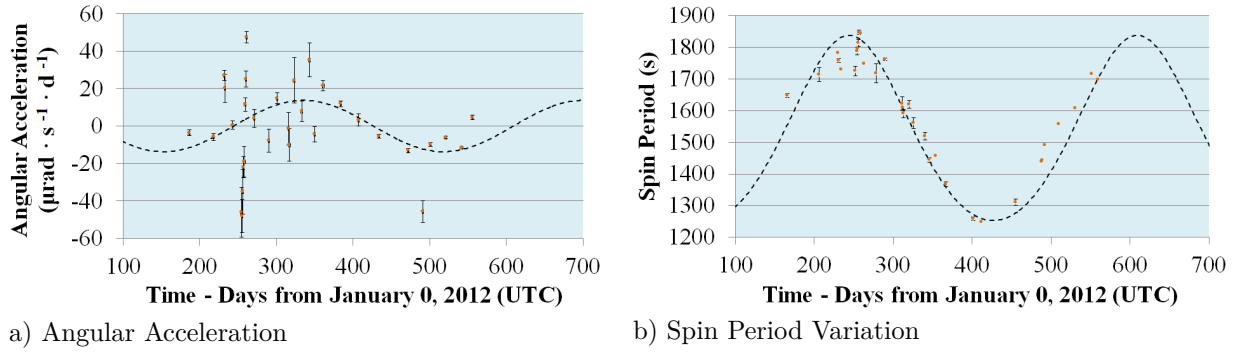


Fig. 14 Comparison of HGS-1's predicted and observed angular acceleration and spin period variation

could also have different relative orientations about their designed rotation axes. As a result, the SRP torque could depend on the reflectivity of four solar panel sides (two per panel) and their relative orientations with respect to the incoming sunlight.

VI. Conclusions

The observed light curves suggested that the RSOs were spinning with unique spin periods with respect to one another. Over a time scale of several days, the spin periods were observed to vary with time, suggesting that an external disturbance torque was being applied to each RSO. Over a time scale of months, the spin periods of Telstar 401 and Echostar 2 were observed to vary in a quasi-periodic fashion. The spin period of Solidaridad 1 was observed to vary more slowly than those of Telstar 401 and Echostar 2. This suggests that if Solidaridad 1's spin period variation is quasi-periodic, then the timescale might be several years rather than the Earth's sidereal orbit period. The spin period variation of HGS-1 appeared more sporadic, but overall it also appeared to vary in a quasi-periodic fashion within an approximately yearly timescale.

The observed spin period variations of Solidaridad 1, Telstar 401, and Echostar 2 revealed an inflection feature, approximately in between the spin period variation extrema. Within each inflection feature, the absolute slope of the variation would decrease for a number of days.

The apparent cyclical behavior of the RSOs' spin period variations suggested that the SRP torque's overall magnitude was varying with time. By assuming that the maximum observed angular acceleration was caused solely by the SRP torque, the reflectivities of HGS-1's deployed solar panel sides were found to differ by less than 1 percent.

The proposed first-order model for HGS-1's angular acceleration does not adequately explain the highly variable angular acceleration variation of HGS-1 within daily and weekly time frames. However, the proposed first-order model for HGS-1's spin period variation might partially explain the potentially periodic spin period variation of approximately one year duration. The model predicts the spin period variation amplitude of HGS-1, but not its possible period, when the absolute reflectivity difference is set to 0.0019 and the phase

parameter is set to -30 days.

References

- [1] Binz, C. R., Davis, M. A., Kelm, B. E., and Moore, C. I., “Optical Survey of the Tumble Rates of Retired GEO Satellites,” *Proceedings of the Advanced Maui Optical and Space Surveillance Technologies (AMOS) Conference*, 2014.
- [2] Galabova, K. K., *Architecting a Family of Space Tugs based on Orbital Transfer Mission Scenarios*, Master’s thesis, Massachusetts Institute of Technology, 2004.
- [3] Pampushev, P., Karavaev, Y., and Mishina, M., “Investigations of the evolution of optical characteristics and dynamics of proper rotation of uncontrolled geostationary artificial satellites,” *Advances in Space Research*, Vol. 43, 2009, DOI: 10.1016/j.asr.2009.02.007, pp. 1416–1422.
- [4] Cognion, R. L., “Rotation rates of inactive satellites near geosynchronous earth orbit,” *Proceedings of the Advanced Maui Optical and Space Surveillance Technologies (AMOS) Conference*, 2014.
- [5] Lanzerotti, L. J., “Space Weather Effects on Technologies,” *Geophysical Monograph Series*, Vol. 125, 2001.
- [6] Choi, H. S., Lee, J., Cho, K. S., Kwak, Y. S., Cho, I. H., Park, Y. D., Kim, Y. H., Baker, D. N., Reeves, G. D., and Lee, D. K., “Analysis of GEO spacecraft anomalies: Space weather relationships,” *Space Weather*, Vol. 9, 2011, DOI: 10.1029/2010SW000597, pp. S06001.
- [7] Kinney, L., Gillen, B., Michalopoulos, P., and Vorwig, P. A., “In the Matter of EHOSTAR CORPORATION: Amendment to Application for New Earth Station Under Call Sign E080120 to Add EchoStar 8 Operating as a Mexican Licensed Satellite at 77° W.L. as a Point of Communication,” July 2008.
- [8] Ocampo, C., “Trajectory analysis for the lunar flyby rescue of Asiasat-3 / HGS-1,” *Annals of the New York Academy of Sciences*, Vol. 1065, December 2005, DOI: 10.1196/annals.1370.021, pp. 232.
- [9] Reddy, M. R., “Space solar cells - tradeoff analysis,” *Solar Energy Materials & Solar Cells*, Vol. 77, 2003, DOI: 10.1016/S0927-0248(02)00320-3, pp. 204.
- [10] Wertz, J. R., Meissinger, H. F., Newman, L. K., and Smit, G. N., *Orbit and Constellation Design and Management*, Microcosm Press and Springer, 2nd ed., 2009.